

RF and Microwave Component Development in LTCC

Liam Devlin, Graham Pearson, Jonathan Pittock
Plextek Ltd, London Road, Great Chesterford Essex, CB10 1NY
Tel. +44 (0)1799 533200, Fax. +44 (0)1799 533201, Email: LMD@PLEXTEK.CO.UK

Bob Hunt, C-MAC Micro Technologies

Abstract

Low Temperature Co-fired Ceramic (LTCC) technology is a multi-layer ceramic process that can be used to fabricate low cost, high performance RF and microwave components. It is an extremely versatile technology that can be used to realise a wide range of components from simple passive filter structures and packages to complex sub-system assemblies containing discrete SMT (Surface Mount Technology) components, bare die and printed passives. This paper presents an overview of the LTCC fabrication process and details an on-going programme of work aimed at providing the detailed RF characterisation data that designers require in order to fully exploit the benefits of the technology. Measured material characterisation data is presented for a number of different LTCC substrate materials and metallisations. Two different band-pass filter structures, one at 2.4GHz the other at 28GHz, have been developed to assess the accuracy of the characterisation data. Details of the design, layout and measured performance of these filters is also presented. Further development work, underway at the time of writing, is also described and results from this will be presented at the conference.

Overview of LTCC Technology

LTCC technology is a multi-layer ceramic process. The ceramic layers are tape-cast in their pre-fired "green-state" and the tape is cut to the required size. Registration holes, via holes and cavities are then punched or drilled into the different tape layers. The via holes are normally filled, often with silver, and then thick film processing is used to print metallisation patterns on each, or selected tapes. When thick film processing is used, the minimum line width/gap is around 100µm. If finer line geometries are required a photo-imagable process can be used [1]. The different layers are then inspected, registered and laminated and then co-fired at around 850°C. Post fired processing of the top layer is also an option that is sometimes used.

This description of the LTCC process makes it sound similar to conventional multi-layer circuit boards fabricated using laminate materials such as FR4. However, LTCC has a number of advantages:

- Lower loss dielectric (lower $\tan\delta$)
- Better controlled dielectric properties (ϵ_r , $\tan\delta$ and thickness)
- It is well suited to producing modules in low-cost SMT packages, including BGA topologies
- LTCC processes can produce modules, which are well suited to incorporating bare die. Cavities and integral heat-sinks can be easily realised
- Many processes allow the integration of printed passive components (resistors, capacitors and inductors)

A 3-dimensional image of an LTCC assembly incorporating a bare die, SMT components and integrated passives is shown in Figure 1.

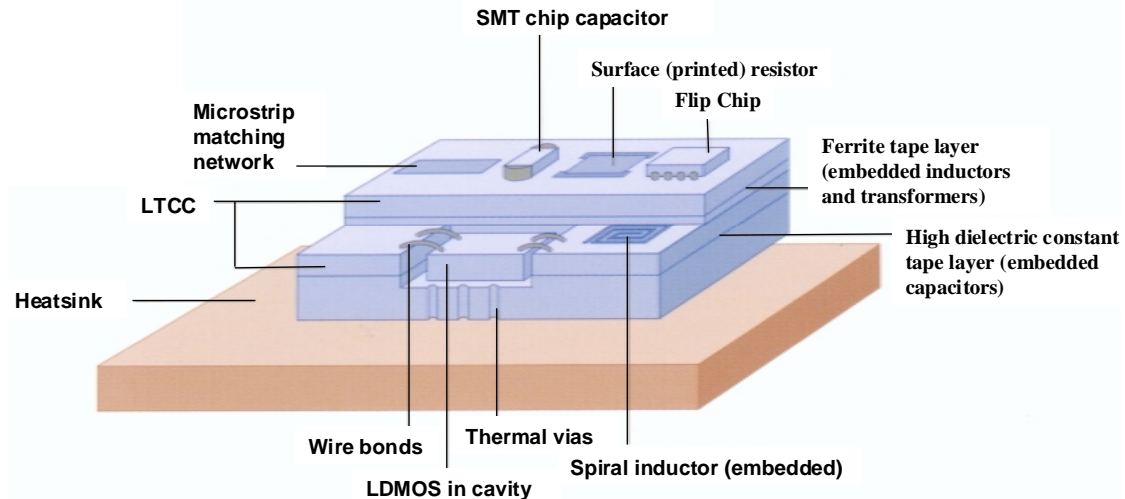


Figure 1: LTCC substrate with integrated passives

Some of the advantages of LTCC listed above (lower $\tan\delta$ and better control of dielectric properties) can also be achieved with traditional thick film processes. In this case it is the other features of LTCC that provide advantages:

- Layers are produced in parallel resulting in reduced costs and increased yields
- There is only a single firing operation (taking around 4 hours) so reducing production time and cost
- Each layer can be inspected prior to stacking, which also improves yield
- Multiple layer structure allows the realisation of innovative printed structures such as baluns and filters [2] and facilitates miniaturisation

There are obviously also perceived disadvantages to LTCC and amongst those cited are:

- Many processes are not mature and much process development is still on-going
- RF characterisation data, for both the integral passive components and the materials themselves, are not readily available
- During the firing process there is tape shrinkage of between 12% and 16% occurs in the X and Y dimensions and slightly more in the Z

The shrinkage is often cited, by proponents of alternative technologies, as the main drawback to using LTCC. However, with well-controlled processes, the shrinkage can be kept within a narrow window, provided the metal loading across the tape is balanced. Some manufacturers are also developing “zero-shrink” LTCC processes.

With respect to the lack of RF characterisation data, the work described here is evidence that work is underway to change this. It should be noted that the difficulties with the availability of comprehensive RF characterisation data, does not mean that LTCC based RF components for volume applications don't exist. Figure 2 shows a power amplifier (courtesy of Ultra RF) for use in base station applications.

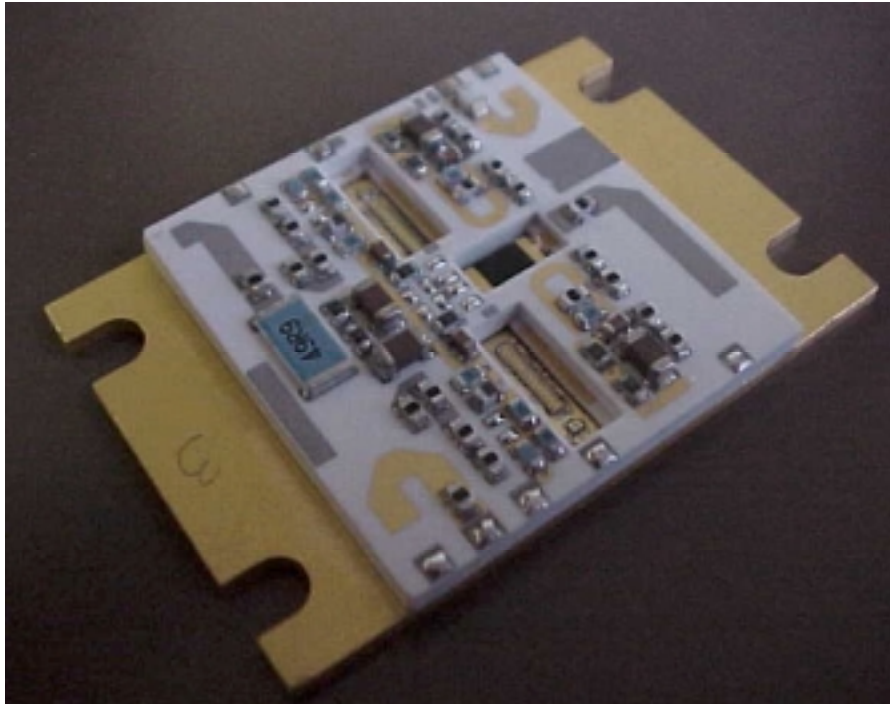


Figure 2: LTCC RF power amplifier module for base station applications (courtesy of Ultra RF)

Material Characterisation

The important material parameters of a substrate material for RF and microwave applications are the dielectric constant (relative permittivity), ϵ_r and the loss tangent (dissipation factor), $\tan\delta$. However, the conductor properties and surface roughness of the substrate material must also be considered for optimum performance/cost tradeoff. Dielectric constant and loss tangent can be determined using a number of different methods as discussed in [3]. The technique selected for the characterisation described here was to fabricate and evaluate microstrip ring resonators [4].

Most RF and microwave LTCC components utilise printed transmission lines and microstrip ring resonators can be conveniently fabricated and measured. Preliminary evaluation data, described in [5], was used as the basis for the ring resonator design. Rings with fundamental resonant frequencies of 1GHz, 2GHz, 3GHz, 4GHz and 5GHz were produced. A photograph of one set of the ring resonators is shown in Figure 3. Also shown in the photograph is a Through Reflect Line (TRL) calibration tile, which is used to calibrate out the effects of the test jig [6]. A photograph of the commercially available test jig, which is suitable for use up to 60GHz, is shown in Figure 4.

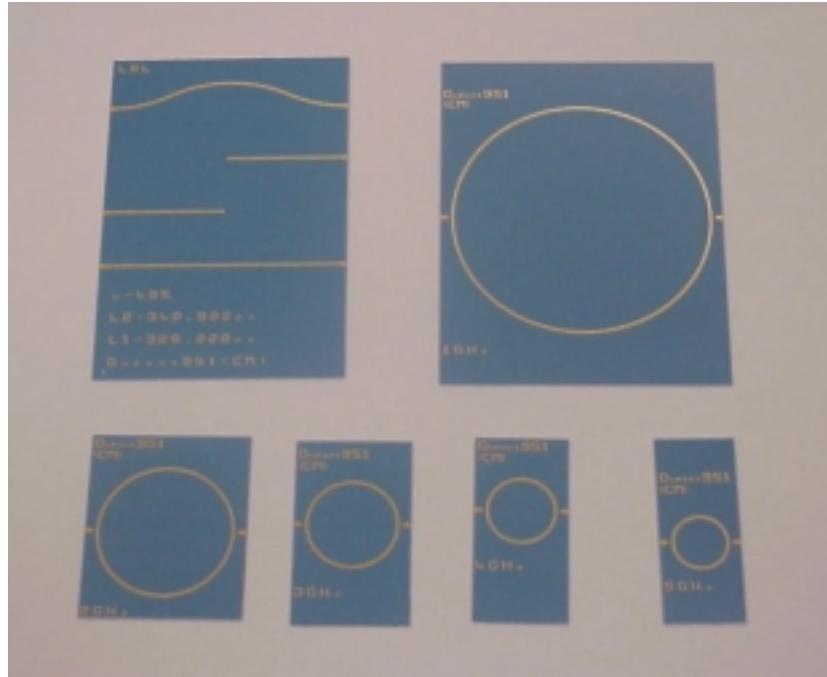


Figure 3: Photograph of the ring resonators and TRL calibration tile



Figure 4: Photograph of test jig

As the fundamental resonant frequency of a ring resonator increases, so the physical size of the ring reduces. As ring resonators get smaller, they can exhibit problems associated with increased radiation and coupling across the ring. In order to avoid such problems 5GHz was the highest fundamental frequency ring that was fabricated. Characterisation data above 5GHz can be obtained by measuring the harmonic resonances of the rings.

It should be remembered that microstrip transmission lines are dispersive. This means that the

(effective) dielectric constant, for signals propagating on the transmission line, varies with frequency. The thicker the substrate the more dispersive it is, which effectively sets an upper limit on substrate thickness and/or maximum operating frequency. All of the ring resonators were fabricated with a substrate thickness of 0.4mm. For the dielectric materials under consideration, microstrip lines on this thickness of substrate can be considered to suffer from negligible dispersion up to around 25GHz.

The test tiles have a short feed line to the ring resonator followed by a gap. Energy is capacitively coupled into the ring resonator and travels around to the output feedline. The coupling between feedline and resonator is very low, which is necessary to ensure the resonator can be considered to be “un-loaded”. There is a peak in transmission from input to output at frequencies where the mean circumference of the ring resonator is an integral number of wavelengths long. All feed lines are kept as small as possible to avoid resonances in the feedlines themselves, which could mask the resonant peaks of the rings.

Characterisation was carried out for the following substrate materials:

- Dupont 951
- Dupont 943

- Ferro A6
- Heraeus CT2000
- C-MAC-9

Two different conductors were considered: gold and silver. The measured insertion loss of all 5 different sizes of resonator is shown in Figure 5 through to Figure 9, for the Dupont 943 substrate with silver metallisation.

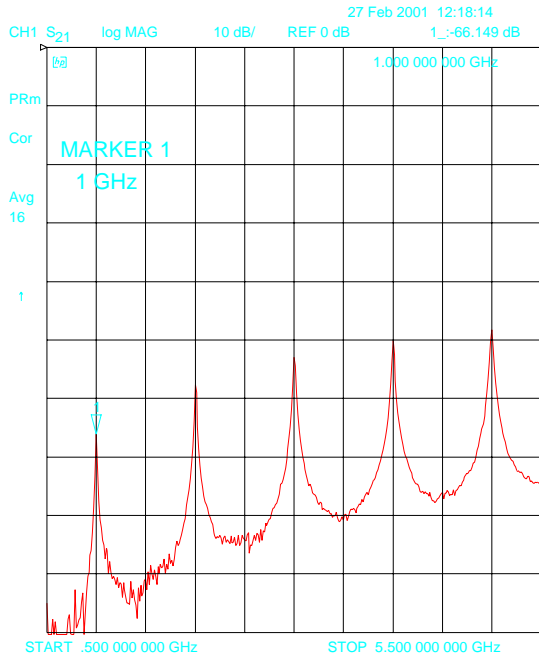


Figure 5: Dupont 943, Ag metallisation, 1GHz resonator

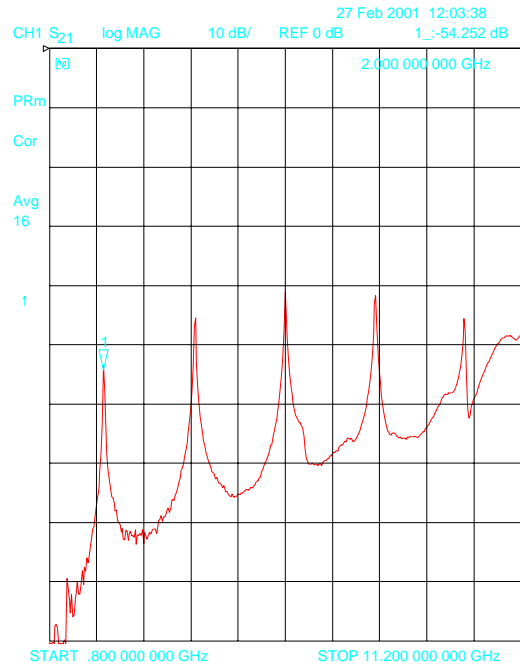


Figure 6: Dupont 943, Ag metallisation, 2GHz resonator

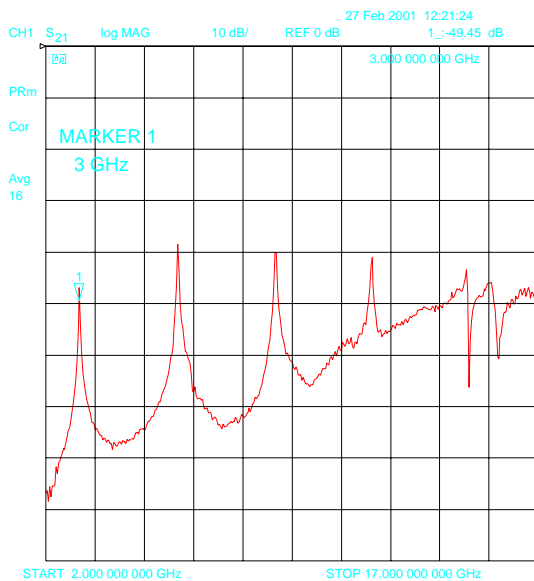


Figure 7: Dupont 943, Ag metallisation, 3GHz resonator

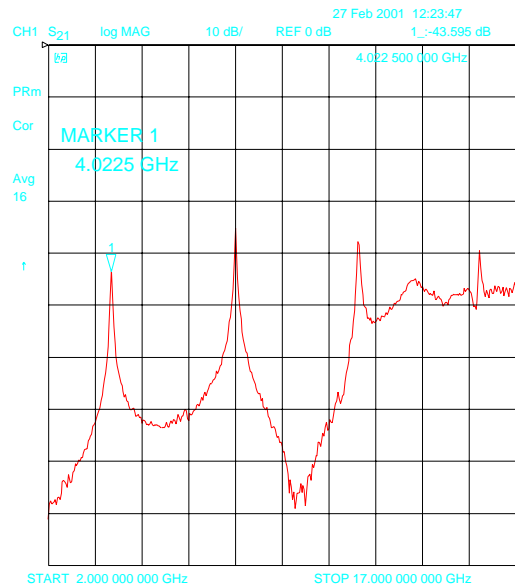


Figure 8: Dupont 943, Ag metallisation, 4GHz resonator

The resonant frequency of the transmission peaks is used to determine the dielectric constant and the Q of the resonance is used to determine the loss tangent. All of the broadband measurements shown above were used merely to investigate the general trend of the resonator response. For the detailed resonant frequency and Q measurements calibration was carried out over a much narrower band as shown in Figure 10. This allows increased frequency resolution. At frequencies above around 12GHz, the resonant peaks are no longer visible. This is a result of the coupling from the input to output feedlines across the jig actually exceeding the coupling through the ring resonator. Thus the resonant peaks of the ring are masked. Alternative structures are currently being investigated to resolve this issue and allow material characteristic to higher frequencies.

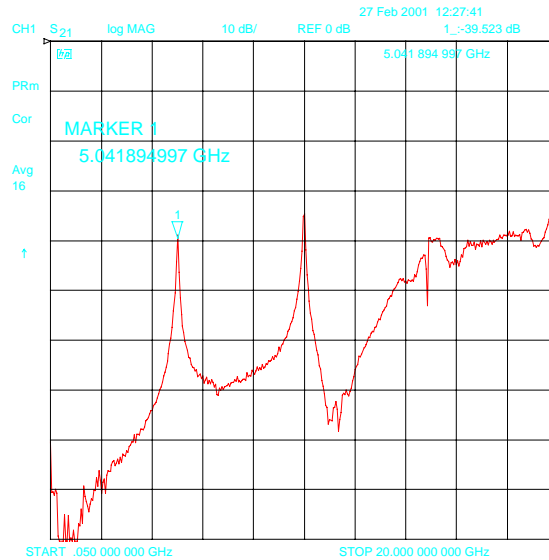


Figure 9: Dupont 943, Ag metallisation, 5GHz resonator

At the fundamental frequency of resonance, the circumference of the resonator is one wavelength long. At the 2nd harmonic it is two wavelengths long and at the 3rd harmonic, three wavelengths long and so on. In all cases the wavelength is the guide wavelength (λ_g) of signals propagating on the microstrip transmission line. Given that the mean circumference of the resonator is known, this allows the effective dielectric constant of the microstrip transmission line to be determined using Equation 1. Where c is the speed of light, F the frequency and λ_g the wavelength.

Equation 1:
$$\epsilon_{eff} = \left[\frac{c}{\lambda_g \cdot F} \right]^2$$

Complex equations are available [7] allowing the relationship between the effective dielectric constant (ϵ_{eff}) and the relative dielectric constant (ϵ_r) to be determined. However modern RF CAD packages have transmission line calculators that allow the value of ϵ_r to be determined much more conveniently and this was the approach adopted for this work.

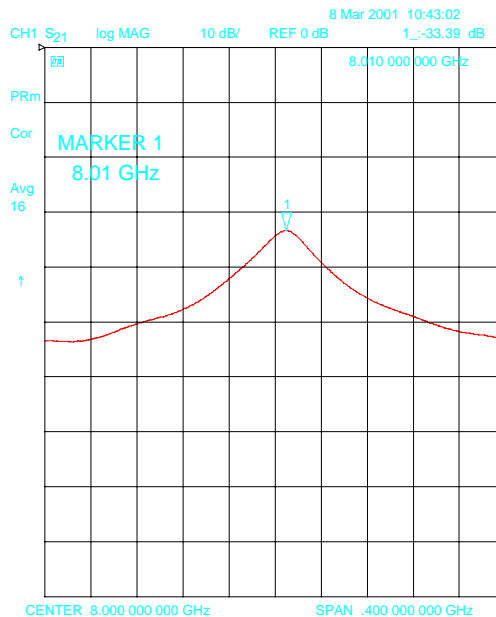


Figure 10: Close-in plot of the 2nd harmonic of the 4GHz resonator on Dupont 943, Ag

The measured ϵ_r (determined as described above) for the Dupont 943 material is plotted against frequency in Figure 11 and Figure 12. Results from all five resonators are plotted on a single graph. One chart is from measurements of the silver resonators, the other from measurements of the gold. The agreement in ϵ_r determined using the two different metallisations is excellent. There is also a very good correlation between the ϵ_r at specific frequencies determined using different resonators.

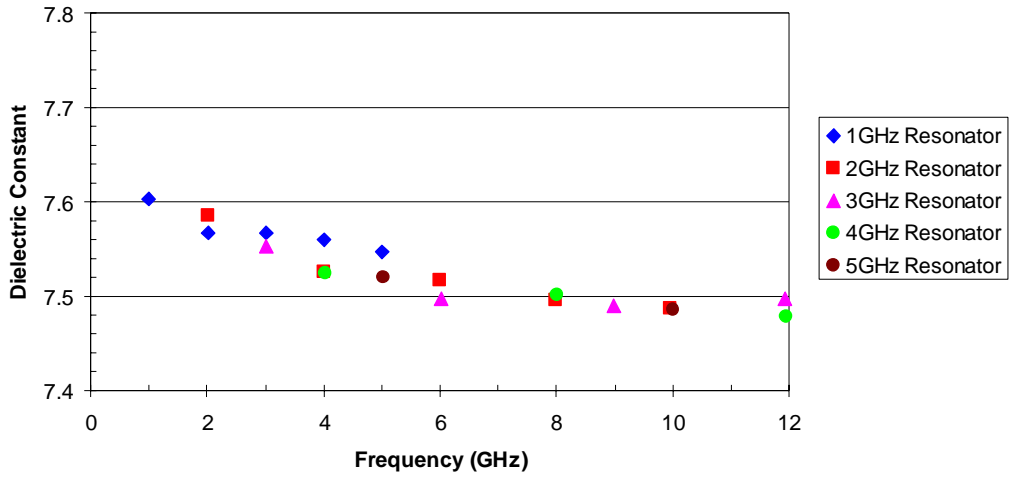


Figure 11: Measured ϵ_r of Dupont 943 from Ag metallisation resonators

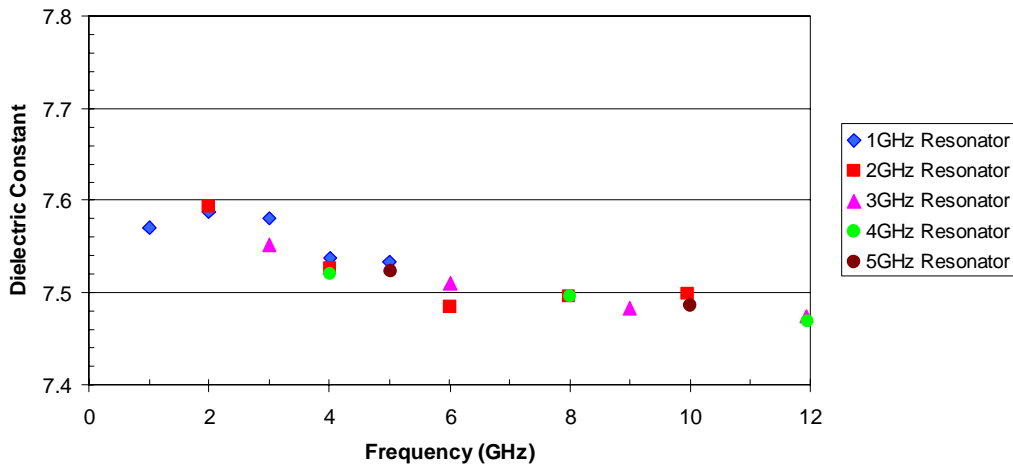


Figure 12: Measured ϵ_r of Dupont 943 from Au metallisation resonators

Results of a similar uniformity were obtained for the other materials investigated. Figure 13 summarises the values of ϵ_r determined for the different materials. The materials in red were as a result of this work, whilst those in blue are as a result of previous investigations [5].

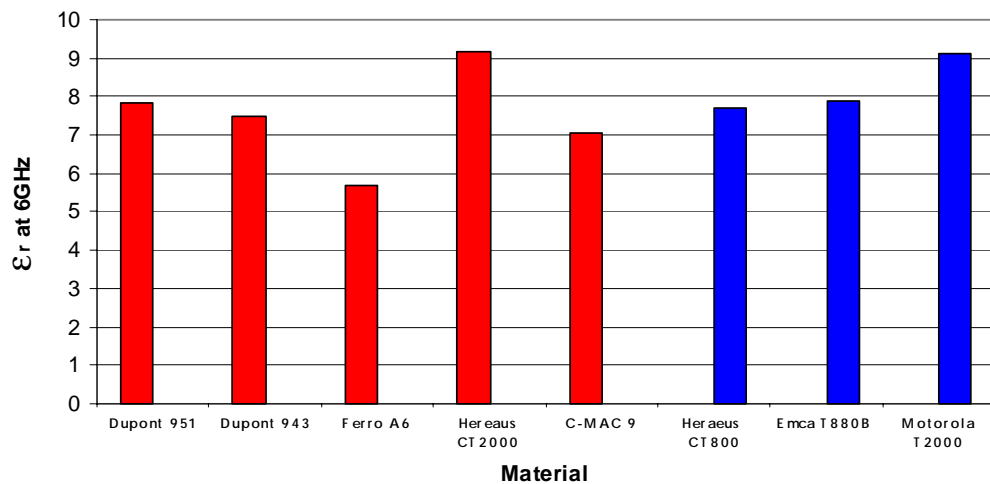


Figure 13: Summary of ϵ_r estimates of materials at 6GHz

The loss tangent of the substrate ($\tan\delta$) can be determined from measurement of the Q factor of the resonators. The Q of the ring resonators is simply the ratio of the centre frequency to the 3dB bandwidth. As the resonators are only very lightly loaded (low coupling into the resonator) the measured Q is the unloaded Q (Q_o). The Q_o of a microstrip line is given by Equation 2, from [7].

$$\text{Equation 2: } Q_o = \frac{\pi}{\alpha \cdot \lambda_g}$$

Where λ_g is the guide wavelength (of the microstrip line) at the frequency of interest and α is the total loss (in nepers per unit length). If losses are split into conductor losses (α_c) and dielectric losses (α_d) then Q_o can be expressed by Equation 3:

$$\text{Equation 3: } \frac{1}{Q_o} = \frac{\alpha_c \cdot \lambda_g}{\pi} + \frac{\alpha_d \cdot \lambda_g}{\pi} = \frac{1}{Q_c} + \frac{1}{Q_d}$$

The loss tangent ($\tan\delta$) is the reciprocal of Q_d , thus we can rearrange Equation 3 to give an expression for $\tan\delta$, as shown in Equation 4:

$$\text{Equation 4: } \tan\delta = \frac{1}{Q_o} - \frac{\alpha_c \cdot \lambda_g}{\pi}$$

Q_c is calculated from the metal properties of the conductor and knowledge of its thickness and surface roughness, which is $0.8\mu\text{m}$. Once again the transmission line calculator of a modern RF CAD package was used as a convenient means of making this calculation.

Figure 14 shows the measured unloaded Q of the silver Ferro A6 resonators versus frequency. The correlation between the unloaded Q of the different resonators at specific frequencies, is very good. Figure 15 is a similar graph for the gold Ferro A6 resonators. The value of the unloaded Q has dropped as a result of the lower conductivity of the gold compared to the silver.

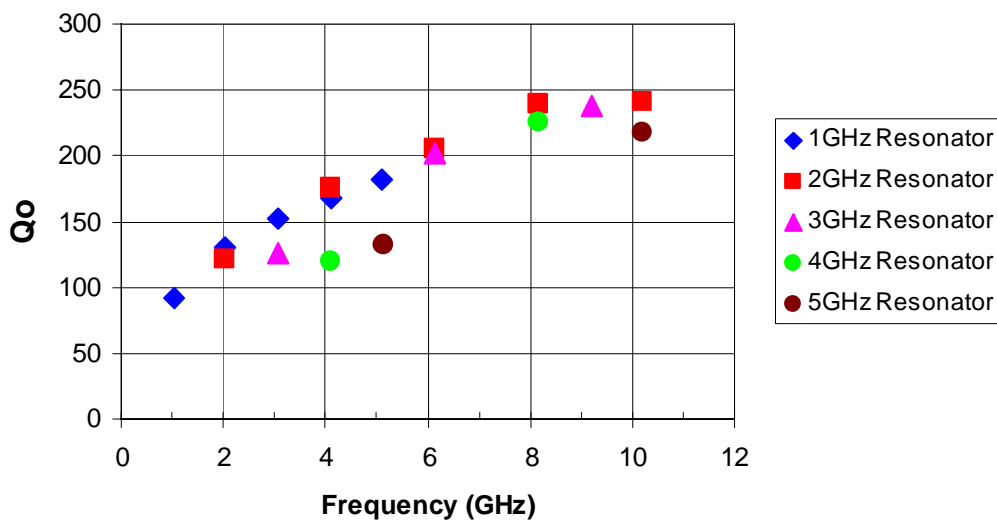


Figure 14: Unloaded Q of Ferro A6 resonators, Ag metallisation

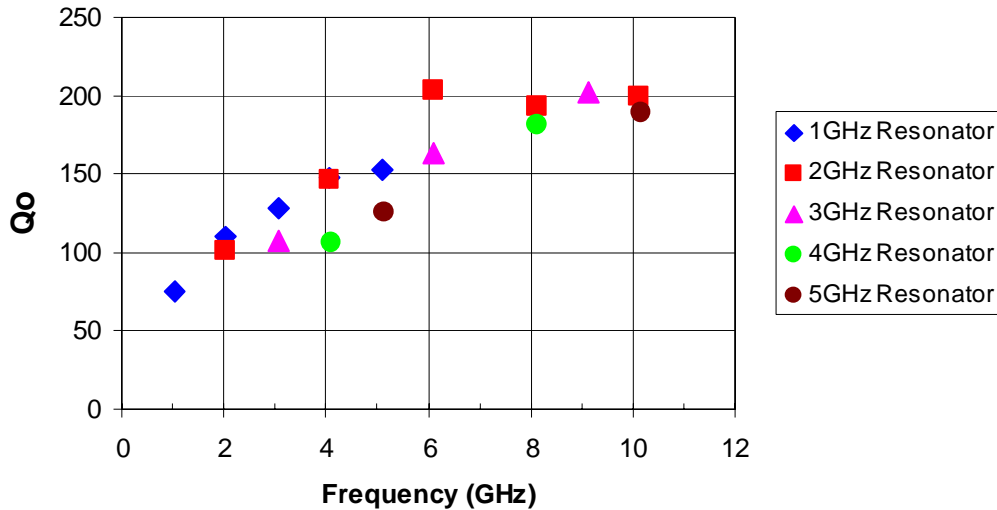


Figure 15: Unloaded Q of Ferro A6 resonators, Au metallisation

The spread in the measured unloaded Q values of Figure 14 and Figure 15 due in part to the variation of conductor width and thickness. This is a limitation of the thick film process. The tolerance on line width is $\pm 12\mu\text{m}$ and the conductor thickness is between $9\mu\text{m}$ and $11\mu\text{m}$. This degree of variation can cause a unit to unit variation in the absolute value of measured Q of around ± 5 . Taking a line of best fit through the measured Q data, the loss tangent versus frequency was determined using the method described above. The resulting loss tangent versus frequency is plotted for the Dupont 951 and Ferro A6 materials in Figure 16. The values determined using both the silver and gold resonators are plotted on the same graph and the agreement is very good. This gives increased confidence in the validity of these results.

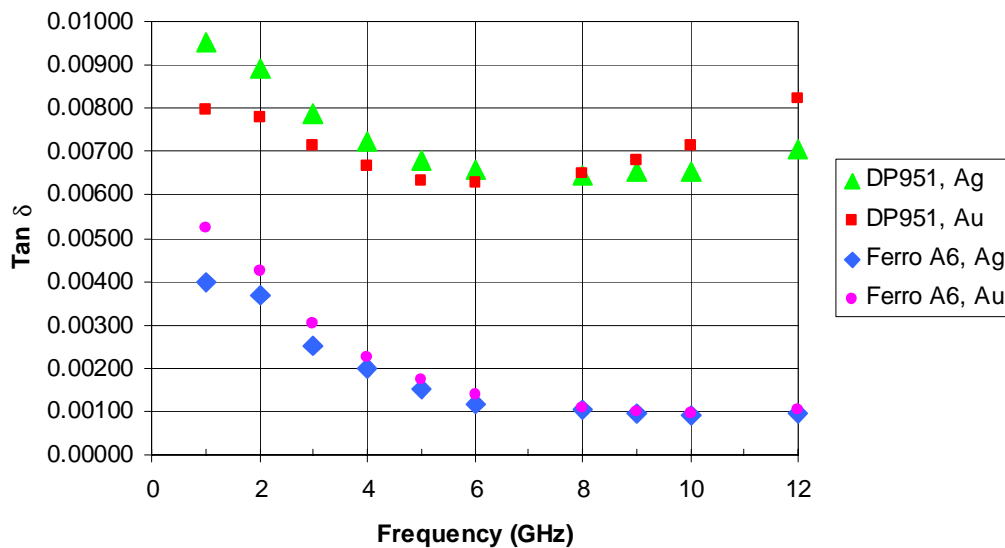


Figure 16: Measured loss tangent for Ferro A6 and Dupont 951 resonators, using Au and Ag resonators

Results of a similar uniformity were obtained for the other materials investigated. Figure 17 summarises the values of $\tan\delta$ determined for the different materials. The materials in red were as a result of this work, whilst those in blue are as a result of previous investigations [5].

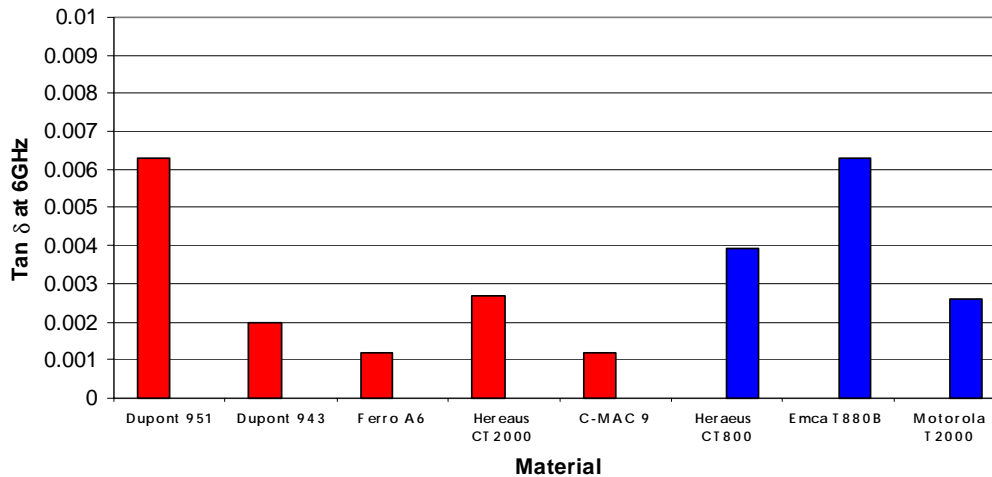


Figure 17: Summary of measured $\tan\delta$ for different materials

In the results described above, the Hereaus CT2000 material is a version of the Motorola T2000 material, cast by Hereaus. Given the fact that these two materials were cast by different companies some 9 months apart in time, the agreement in the values determined for both $\tan\delta$ (Figure 13) and ϵ_r (Figure 17) is excellent.

RF and Microwave Component Realisation

Two band-pass filters have been designed for a range of the LTCC tape systems. One of these addresses the Bluetooth/ISM frequency band from 2.4 to 2.483GHz. The other is a mm-wave design centred on 28GHz.

Bluetooth/ISM Filter

Filters for the 2.4GHz ISM/Bluetooth frequency band were designed for several of the different material systems. The design is a three-section capacitively loaded tapped combline type. A photograph of one of the filters is shown in Figure 18. The design uses 0402 ceramic SMT capacitors, which are attached to the completed LTCC tile using solder or conductive epoxy. To accurately simulate the performance of this filter it is necessary to include the parasitics of the SMT capacitors and the LTCC vias to ground.

Figure 19 shows the measured performance of one of the filters on the Dupont 943 substrate material with gold conductor. Figure 20 is the same filter on the same substrate material but using silver conductor. The increased conductivity of the silver metallisation can be seen to reduce the band centre loss from 1.2dB to 1.0dB. These losses also include the 50 Ω input and output track to the filter.

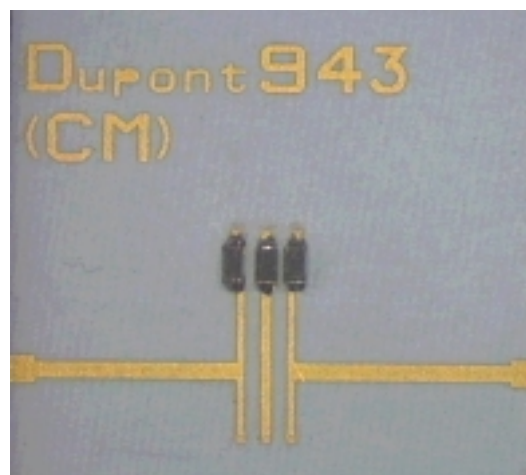


Figure 18: Photograph of the 2.4GHz BPF (overall tile width =15mm)

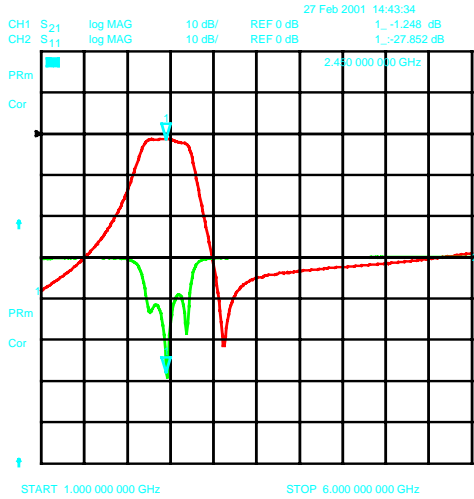


Figure 19: Measured performance of Dupont 943, 2.4GHz BPF, Au metal

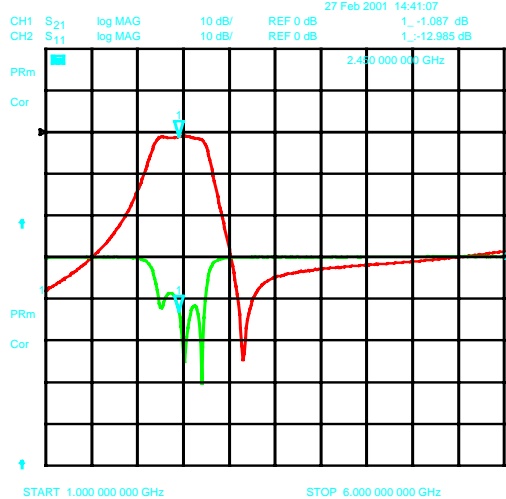


Figure 20: Measured performance of Dupont 943, 2.4GHz BPF, Ag metal

A comparison of the measured and modelled performance is shown for the Dupont 943 filter using Au metallisation in Figure 21. All filters exhibited a slightly wider than simulated bandwidth. This is likely to be a result of processing tolerance resulting in a smaller than designed coupling gap. If this sort of variation could not be tolerated in practice, an photo-defined top layer metallisation pattern could be used to give improved definition.

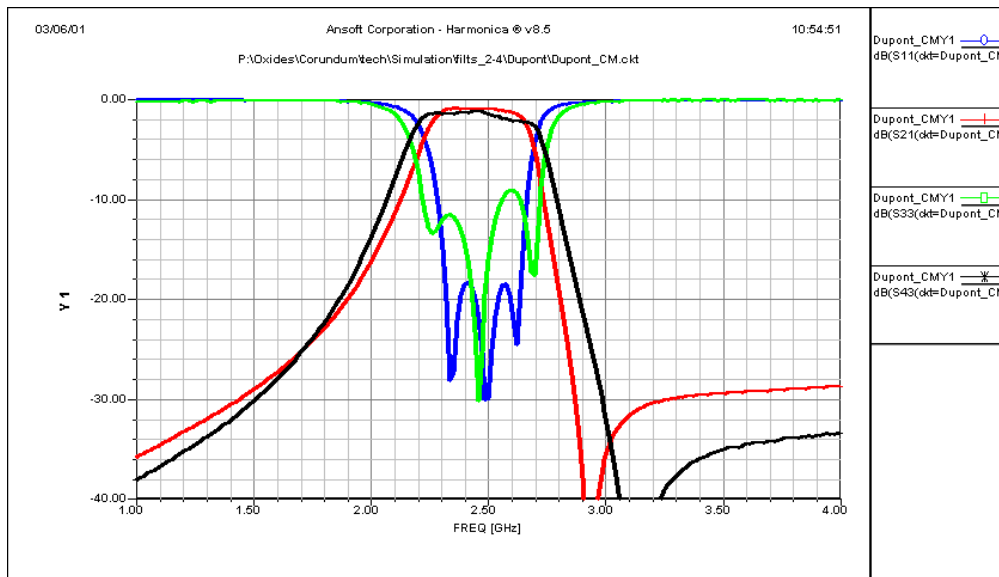


Figure 21: Comparison of measured to simulated performance of Dupont 943, 2.4GHz BPF, Au metallisation

MM-Wave Filter

A popular printed filter topology at microwave and mm-wave frequencies is the edge-coupled filter. A four section, 28GHz version of such a filter has been designed in a number of the tape materials. It would find use in applications such as broadband wireless communications. A photograph of one of the filters is shown in Figure 22. The wide lengths of line at the input and output to the filter are impedance matching sections, which help to ease the requirements for narrow track and gap widths within the filter. The minimum line width and spacing used was $160\mu\text{m}$, which can be conveniently fabricated using thick film processing. The overall size was approximately $3\text{mm} \times 6\text{mm}$, depending upon substrate material.



Figure 22: Photograph of one 28GHz BPF (overall tile width =15mm)

The measured versus modelled performance for one of the 28GHz filters is shown in Figure 23. The design is on frequency with an insertion loss of just under 1.5dB, slightly lower than simulated.

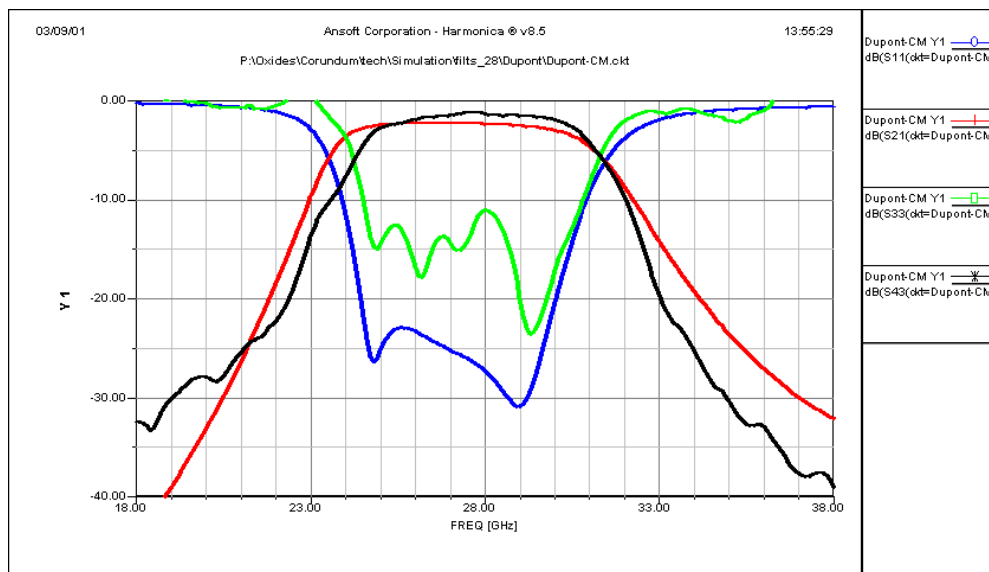


Figure 23: Measured versus simulated performance of mm-wave filter in Dupont 951, silver metallisation

Future Work

As part of the on-going development and demonstration of the LTCC processes, several other components have been designed and are currently being manufactured. These include additional edge-coupled bandpass filters at 28GHz and 42GHz, as shown in Figure 24.

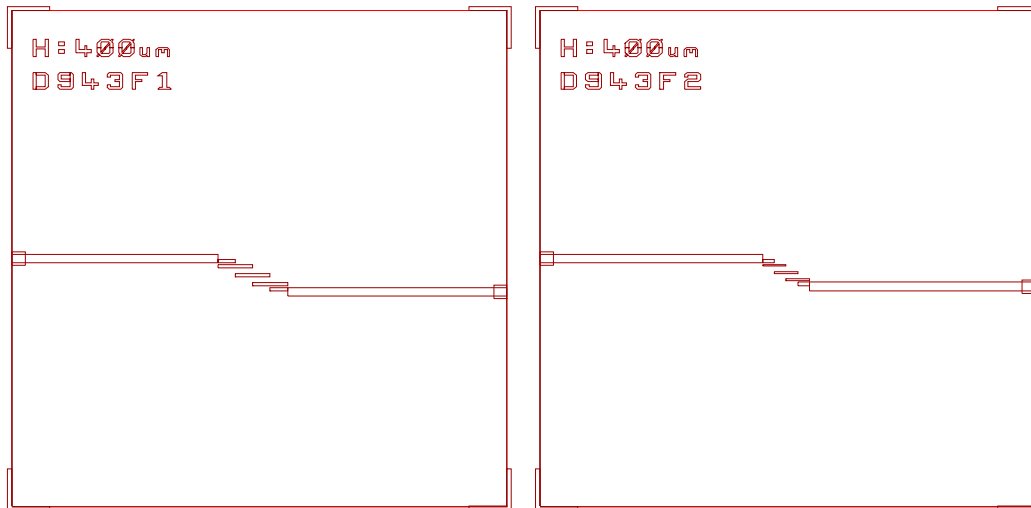


Figure 24: Layout of 28GHz and 42GHz coupled line filters

Broadband -3dB Lange coupler structures, covering 22 to 35GHz, have also been designed. These contain a printed 50Ω resistor to terminate the isolated port and make use of photo-definable metallisation to realise the tight coupling gap ($25\mu\text{m}$) required to achieve the desired performance. The layout for the Lange coupler test tile is shown in Figure 25. It also contains a test pattern in the bottom left hand corner, to allow evaluation of the accuracy of the fine geometry metal definition. A separate version of the isolated port terminating resistor is included to allow evaluation the quality of the match presented to the isolated port.

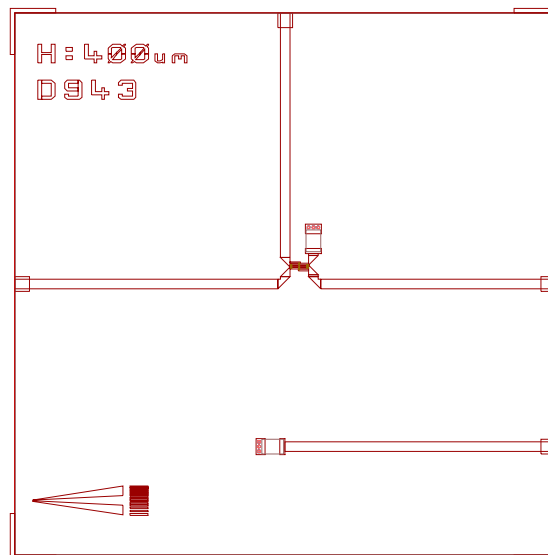


Figure 25: Layout of the 22GHz to 35GHz Lange coupler

A close-in image of the Lange coupler is shown in Figure 26. Also shown are the bond wires that are used to link together the multiple coupled lines of the interdigitated coupling structure.

In order to allow visual evaluation of the quality of the fine geometry metal definition, made possible by the use of a photo-definable top layer metallisation, the test structure shown in Figure 27 has been included on the Lange coupler test tile. This includes parallel and tapered lines down to track and gap geometries of $25\mu\text{m}$.

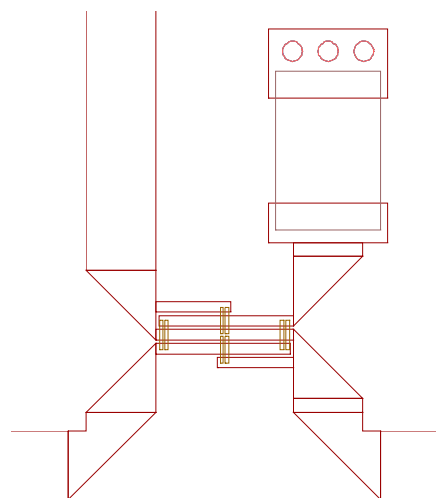


Figure 26: Close-in of layout detail of the 22GHz to 35GHz Lange coupler

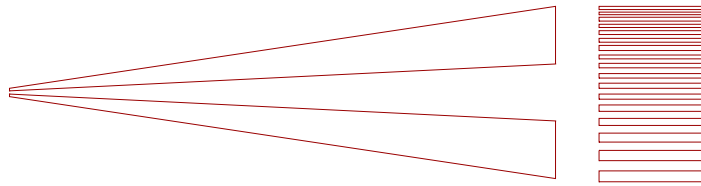


Figure 27: Close-in of metal definition test pattern

Conclusions

LTCC is well suited to realising compact, multi-function RF and microwave modules. These can include, bare die, SMT components and printed passives such as filters, couplers and baluns. The technology is capable of low cost, high volume manufacture.

This paper has presented material characterisation techniques and measured results for a number of LTCC tape materials. It has also detailed the design and measured performance of 2.4GHz and 28GHz band-pass filters. A comparison of the material properties of a range of LTCC tape systems and some well-known, commercially available RF and microwave substrate materials is presented in Table 1.

Material	ϵ_r	Tan δ
FR4	4*	0.025
Rogers RO4003	3.38 \pm 0.05	0.0027
Rogers RT/Duroid 5880	2.20 \pm 0.02	0.0009
99.6% Alumina	9.9	0.0004
Dupont 951	7.85	0.0063
Dupont 943	7.5	0.002
Ferro A6	5.7	0.0012
Heraeus CT2000	9.15	0.0027
C-MAC-9	7.05	0.0012
Heraeus CT800	7.68	0.0039
Emca T880B	7.94	0.0063
Motorola T2000	9.09	0.0026

*Varies significantly from supplier to supplier

Table 1: Summary of substrate material properties

Although the LTCC materials don't exhibit the very low loss tangents of high purity ceramics they are never the less, low loss materials. This fact combined with the advantages of the multi-layer structure, printed passives and low cost processing mean that LTCC has much to offer for the realisation of RF and microwave components.

References

- [1] Scramton, C.Q. and Lawson, J.C., "LTCC Technology: Where we are and where we're going to", Proceedings of the IEEE MTT-S International Topical Symposium for Wireless Applications, Feb. 1999, pp 193-200
- [2] Sheen, J-W., "LTCC-MLC Duplexer for DCS-1800", IEEE MTT-Transactions, Vol. 47, No. 9, Sept. 1999, pp. 1883-1889
- [3] James Baker-Jarvis, Bill Riddle and Michael D. Janezic, "Dielectric and Magnetic Properties of Printed Wiring Boards and Other Substrate Materials", National Institute of Standards and Technology (NIST), Technical Note 1512, March 1999

- [4] Mayercik, M.E., "Resonant Microstrip Rings and Dielectric Material Testing", *Microwaves & RF*, April 1991, pp. 95-102
- [5] Liam Devlin, Graham Pearson and Bob Hunt, "Low Cost RF and Microwave Components in LTCC", *Proceedings of MicroTech 2001*, January 2001, pp 59-64
- [6] Hewlett Packard Product Note 8510-8, "Network Analysis, Applying the HP8510B TRL calibration for non-coaxial measurements"
- [7] Edwards, Terry, "Foundations for Microstrip Circuit Design", John Wiley & Sons, 1992, ISBN 0-471-93062-8